Optimization of Conical Intersections Using the Semiempirical MNDOC–CI Method with Analytic Gradients

ROBERTO IZZO, MARTIN KLESSINGER

Organisch-Chemisches Institut der Westfälischen Wilhelms-Universität, D-48149 Münster, Germany

Received 16 June 1999; accepted 19 August 1999

ABSTRACT: An efficient procedure is presented for calculating analytic gradients in the framework of a semiempirical multireference configuration interaction method. The same algorithm is used to locate the lowest energy point of a conical intersection by the direct method of Bearpark et al. (Chem Phys Lett 1994, 223, 269). Results for the conical intersections on the photoreactions of ethylene and butadiene are in very good agreement with *ab initio* data. In addition, conical intersections were optimized of the photoreactions of azirine as well as for the cyclooctatetraen–semibullvalene and the dewarnaphthalene–naphthalene photorearrangement reactions.
 J Comput Chem 21: 52–62, 2000

Keywords: analytic gradients; conical intersections; multireference CI; photoreactions; semiempirical

Introduction

Recent experimental results[1, 2] and new computational methods[3, 4] have provided a new mechanistic picture of photochemical reactions,[5] which can be understood in terms of the evolution of an excited-state species toward a conical intersection that acts as a photochemical decay channel. Although under certain conditions the shape of the excited-state potential energy surface is expected to play a dominant role in determining the ultrafast dynamics on this surface, detailed information on the reaction rate and photoproduct distribution requires quantum or semiclassical dynamics computations.[4] However, even for medium-size molecules the high computational cost renders the use of such methods difficult, because quantum chemical calculations for photochemical reactivity problems are rather demanding inasmuch as static as well as dynamic correlation effects are of uppermost importance and larger basis sets including diffuse functions are required to yield accurate results.[6]

In our previous work on excited-state reactivity[7, 8] the semiempirical MNDOC–CI method (**m**odified **n**eglect of **d**iatomic **o**verlap parametrized

Dedicated to Prof. Josef Michl on the occasion of his 60th birthday.

Correspondence to: M. Klessinger; email: klessim@uni-muenster.de

Contract/grant sponsor: Deutsche Forschungsgemeinshaft, Bonn, and Fonds der Chemischen Industrie, Frankfurt

CCC 0192-8651 / 00 / 010052-11

for taking into account **c**orrelation effects explicitly by **c**onfiguration **i**nteraction)[9] has proven very useful in exploring excited-state geometries and potential energy surfaces prior to the application of *ab initio* methods to get the final results. The MNDOC–CI method is based on spin-adapted CSFs (**c**onfigurational **s**tate **f**unctions), and includes selected single and double excitations with respect to one or several reference configurations within an active space of commonly 10–12 orbitals involved in the process under consideration.[10] Typically, several hundred configurations are included in the CI. Excited-state potential energy surfaces obtained by this method are in surprisingly good qualitative agreement with elaborate *ab initio* results, and geometries of characteristic points are reproduced very well, while quantitative energetic data like excitation energies or barrier heights are somewhat less reliable.[7,8]

We now extended our MNDOC–CI program by introducing the possibility for optimizing and characterizing the lowest point of a conical intersection.[3] Such an optimization procedure requires the local evaluation of the gradients, i.e., the use of analytic gradients, because numerical gradients will cause difficulties because, strictly speaking, the gradient does not exist at the tip of a cone, as well as due to orbital crossing at this point. The new features of the program considerably increase its applicability and usefulness, as they allow for a very fast optimization of stationary points as well as conical intersections even for larger molecules. Such results may serve as initial data for *ab initio* optimizations of conical intersections, and structural effects or substituent effects on the energy and geometry of a conical intersection can be studied with comparatively little effort. On the other hand, analytic gradients within the framework of semiempirical multireference (MR) CI calculations will provide the necessary tools for carrying out semiempirical direct dynamics simulations and trajectory calculations[4,11] for excited-state reactions, in a similar way as semiempirical methods have been used successfully for ground-state reactions.[12] Such investigations will be of particular value in discussing general problems like the influence of barriers on excited-state lifetimes and the accessibility of conical intersections, while the accuracy of the results is, in general, expected not to be sufficient for a comparison with specific experiments.

In the present article we briefly discuss the method we use to calculate analytic gradients within the semiempirical MR–CI approach, and how the same method can be used to optimize conical intersections. We then give a short overview of the implementation and the performance of the program, and, finally, we present the results for the conical intersections of some 10 different photoreactions. Excited-state trajectory calculations will be reported in a forthcoming article.

Theoretical Background

OPTIMIZATION OF CONICAL INTERSECTIONS

A conical intersection is defined as follows: Two states A and B, even if they have the same symmetry, intersect along an $(F-2)$-dimensional hyperline as the energy is plotted against the F nuclear coordinates ($F = 3N_{\text{atom}} - 6$). While for any point in the $(F-2)$-dimensional intersection space the two states are degenerate, the degeneracy is lifted along the two remaining linearly independent coordinates $\mathbf{x}_1$ and $\mathbf{x}_2$. Thus, when the energy of the two states is plotted against these two geometrical variables, the corresponding energy surfaces have the shape of a double cone. In the usual adiabatic electronic representation $\mathbf{x}_1$ is the gradient difference vector and $\mathbf{x}_2$ is parallel to the nonadiabatic coupling element between the two states.[5]

The method for the optimization of the lowest energy point of a conical intersection that we use here is due to Bearpark et al.;[3] it is a direct method, that avoids the use of Langrangian multipliers. The optimization is achieved by simultaneously minimizing the energy difference $E^A_{\text{tot}} - E^B_{\text{tot}}$ in the plane spanned by $\mathbf{x}_1$ and $\mathbf{x}_2$, and minimizing E^B_{tot} in the remaining $(F-2)$-dimensional space orthogonal to the $\mathbf{x}_1, \mathbf{x}_2$ plane.

The condition for the minimization of $E^A_{\text{tot}} - E^B_{\text{tot}}$ in the $\mathbf{x}_1, \mathbf{x}_2$ plane is fulfilled by the gradient

$$\mathbf{f}_1 = 2\big(E^A_{\text{tot}} - E^B_{\text{tot}}\big)\frac{\mathbf{x}_1}{|\mathbf{x}_1|}, \tag{1}$$

while the projection of the gradient of E^B_{tot} onto the $(F-2)$-dimensional complement to the $\mathbf{x}_1, \mathbf{x}_2$ plane

$$\mathbf{f}_2 = \mathbf{P}\frac{\partial E^B_{\text{tot}}}{\partial \mathbf{q}}, \tag{2}$$

is used to fulfill the second condition. If $\tilde{\mathbf{x}}_1$ and $\tilde{\mathbf{x}}_2$ denote the vectors $\mathbf{x}_1$ and $\mathbf{x}_2$ after orthonormalization, the projection matrix $\mathbf{P}$ is given as

$$\mathbf{P} = \mathbf{1} - \tilde{\mathbf{x}}_1\tilde{\mathbf{x}}_1^{\mathrm{T}} - \tilde{\mathbf{x}}_2\tilde{\mathbf{x}}_2^{\mathrm{T}}, \tag{3}$$

where $\mathbf{1}$ is the unit matrix.

The linear combination

$$\mathbf{g} = \alpha_0\big[\alpha_1\mathbf{f}_1 + (1-\alpha_1)\mathbf{f}_2\big], \qquad \alpha_0 > 0,\ 0 < \alpha_1 \leqq 1, \tag{4}$$

is employed for the optimization. $\mathbf{f}_1$ vanishes as soon as degeneracy is reached, and $\mathbf{f}_2$ will decrease the energy within the intersection space. The parameters α_0 and α_1 are kept constant during the optimization; α_1 determines the relative weight of the two partial gradients, while the step size may be manipulated by α_0.

The quasi-Newton algorithm is used for optimization, with the BFGS scheme[13] for updating the Hessian $\mathbf{H}_i$. Starting with the unit matrix for $\mathbf{H}_0$, the gradient $\mathbf{g}_0$ is calculated from eq. (4) at the initial geometry $\mathbf{q}_0$, and the step width δ_0 is calculated from the Newton equation

$$\delta_i = -(\mathbf{H}_i)^{-1}\mathbf{g}_i. \tag{5}$$

If this step is larger than a given radius R, it is rescaled according to

$$\delta_i \rightarrow \frac{r}{|\delta_i|}\delta_i, \qquad 0 < r \leqq R. \tag{6}$$

At the new geometry $\mathbf{q}_1$ the gradient is recalculated yielding $\mathbf{g}_1$, and δ_0 together with the gradient difference $\mathbf{g}_1 - \mathbf{g}_0$ are used to update $\mathbf{H}_1$ for the next cycle, which yields δ_1 from eq. (5), etc. This procedure is repeated until the norm or the RMS value of the projected gradient $\mathbf{f}_2$, respectively, is smaller than a given limit S.

The important input data for the optimization are $\mathbf{x}_1$, $\mathbf{x}_2$, and the energy gradient $\partial E^B_{\text{tot}}/\partial \mathbf{q}$ of the excited state B. As $\mathbf{x}_1$ is the gradient difference, $\mathbf{x}_2$ is the transition gradient with respect to the two states A and B, all these quantities can be determined by the same algorithm, as will be shown below.

ENERGY GRADIENTS

Analytic energy gradients for semiempirical MNDO-type methods have recently been derived by Patchkovskii and Thiel[14, 15] for small single-reference CI expansions, based on a expression for the matrix elements of the CI Hamiltonian in terms of the energy of the reference state, orbital energies, and the corresponding two-electron integrals.[16] As it is essential for applications to excited states to use an MR-CI method, we follow here the more general strategy described by Yamaguchi et al.[17] and express the CI matrix elements as sums over all one- and two-electron integrals multiplied with the corresponding coupling coefficients.

In conformity with the ZDO approximation the basis AOs χ_μ are assumed to be orthonormal, the overlap integrals are

$$S_{\mu\nu} = \int \chi^*_\mu(1)\chi_\nu(1)\, dr_1 = \delta_{\mu\nu}. \tag{7}$$

Thus,

$$\partial S_{\mu\nu}/\partial q_a = 0, \tag{8}$$

where q_a is one of the nuclear coordinates. Furthermore, we assume that configurations are built up from closed-shell SCF-MOs

$$\phi_i = \sum_{\mu}^{\text{AO}} c_{\mu i}\chi_\mu,$$

which in the ground configuration Φ_0 are either doubly occupied (d.o.) or empty.

For orthogonal configurations, the electronic part of the CI gradient is given[17] as

$$\frac{\partial E_{\text{elec}}}{\partial q_a} = \sum_{ij}^{\text{MO}} Q_{ij}h^a_{ij} + \sum_{ijkl}^{\text{MO}} G_{ijkl}(ij|kl)^a + 2\sum_{i>j}^{\text{MO}} F^a_{ij}Z_{ij}. \tag{9}$$

In this equation $\mathbf{Q}$ and $\mathbf{G}$ are the one- and two-electron reduced density matrices[18] and

$$h^a_{ij} = \sum_{\mu\nu}^{\text{AO}} c_{\mu i}c_{\nu j}\frac{\partial h_{\mu\nu}}{\partial q_a} \tag{10}$$

with $h_{\mu\nu} = \langle\chi_\mu|\hat{h}|\chi_\nu\rangle$, and

$$(ij|kl)^a = \sum_{\mu\nu\rho\sigma}^{\text{AO}} c_{\mu i}c_{\nu j}c_{\rho k}c_{\sigma l}\frac{\partial(\mu\nu|\rho\sigma)}{\partial q_a} \tag{11}$$

with $(\mu\nu|\rho\sigma) = \langle\mu\rho|\hat{g}|\nu\sigma\rangle$ are the skeleton (core) derivatives of the one- and two-electron integrals $h_{ij} = \langle\phi_i|\hat{h}|\phi_j\rangle$ and $(ij|kl) = \langle\phi_i\phi_k|\hat{g}|\phi_j\phi_l\rangle$, respectively. The third term in eq. (9) describes the response of the MOs to the nuclear displacements, which is not contained in the skeleton (core) parts; it consists of the skeleton (core) first derivative of the Fock matrix

$$F^a_{ij} = h^a_{ij} + \sum_{k}^{\text{d.o.}}\left[2(ij|kk)^a - (ik|jk)^a\right] \tag{12}$$

and the $\mathbf{Z}$ vector[19] with elements Z_{ij}, which is the solution of the coupled perturbed Hartree–Fock equations (CPHF). This set of equations splits[20] into subset I of pairs of MOs ij with identical occupancies

$$\boldsymbol{\Delta}^{\text{I}}\mathbf{Z}^{\text{I}} = \tilde{\mathbf{X}}^{\text{I}} \tag{13}$$

and subset II of pairs of MOs with different occupancies

$$\left(\boldsymbol{\Delta}^{\text{II}} - \boldsymbol{\alpha}^{\text{II,II}}\right)^{\text{T}}\mathbf{Z}^{\text{II}} = \tilde{\mathbf{X}}^{\text{II}} + \boldsymbol{\alpha}^{\text{II,I}}\mathbf{Z}^{\text{I}} \tag{14}$$

where Δ is the diagonal super-matrix with elements

$$\Delta_{ij,kl} = \delta_{ik}\delta_{jl}(\varepsilon_j - \varepsilon_i) \tag{15}$$

where $\varepsilon_i = \langle\phi_i|\hat{F}|\phi_i\rangle$ is the orbital energy of MO ϕ_i, and $\boldsymbol{\alpha}$ is a nonsymmetric supermatrix given by

$$\alpha_{ij,kl} = 4(ij|kl) - (ik|jl) - (il|jk). \tag{16}$$

The vector $\tilde{\mathbf{X}}$ is defined as $\tilde{X}_{ij} = X_{ij} - X_{ji}$, where

$$X_{ij} = \sum_{m}^{\mathrm{MO}} Q_{jm} h_{im} + 2 \sum_{mkl}^{\mathrm{MO}} G_{jmkl}(im|kl) \qquad (17)$$

is an element of the Lagrange matrix. Subset II [eq. (14)] requires the solution $\mathbf{Z}^{\mathrm{I}}$ of subset I, but not vice versa. Numerical instabilities due to a vanishing energy denominator do not occur in solving the CPHF equations; that is so because they have to be solved only for CI nonredundant pairs of orbitals.[21] In calculations that are physically meaningful, such pairs cannot be degenerate.

Although the CPHF equations are solved in the MO basis, the energy gradient eq. (9) should preferably be evaluated in an AO basis particularly for larger numbers of configurations. Although the transformation of the first two sums in eq. (9) is straightforward (ref. 14), the transformation of the response term [the third sum in eq. (9)] yields

$$\begin{aligned} 2 \sum_{i>j}^{\mathrm{MO}} F_{ij}^{a} Z_{ij} = {} & 2 \sum_{\mu \geq \nu}^{\mathrm{AO}} \left(1 - \frac{\delta_{\mu\nu}}{2}\right) \tilde{Z}_{\mu\nu} \frac{\partial h_{\mu\nu}}{\partial q_a} \\ & + 2 \sum_{\substack{\mu \geq \nu,\ \rho \geq \sigma \\ \mu\nu \geq \rho\sigma}}^{\mathrm{AO}} \left(1 - \frac{\delta_{\mu\nu}}{2}\right)\left(1 - \frac{\delta_{\rho\sigma}}{2}\right)\left(1 - \frac{\delta_{\mu\nu,\rho\sigma}}{2}\right) \\ & \times \left\{4\left[\tilde{Z}_{\mu\nu} D_{\rho\sigma} + \tilde{Z}_{\rho\sigma} D_{\mu\nu}\right] \right. \\ & \left. - \left[\tilde{Z}_{\mu\rho} D_{\nu\sigma} + \tilde{Z}_{\mu\sigma} D_{\nu\rho} + \tilde{Z}_{\nu\rho} D_{\mu\sigma} + \tilde{Z}_{\nu\sigma} D_{\mu\rho}\right]\right\} \\ & \times \frac{\partial(\mu\nu|\rho\sigma)}{\partial q_a} \end{aligned} \qquad (18)$$

where $\tilde{Z}_{\mu\nu} = Z_{\mu\nu} + Z_{\nu\mu}$, and the $\mathbf{Z}$ vector in AO basis is given by

$$Z_{\mu\nu} = \sum_{i>j}^{\mathrm{MO}} c_{\mu i} c_{\nu j} Z_{ij}, \qquad (19)$$

$\mathbf{D}$ is the SCF density matrix with elements

$$D_{\mu\nu} = \sum_{k}^{\mathrm{d.o.}} c_{\mu k} c_{\nu k} \qquad (20)$$

and the superindices $\mu\nu$ and $\rho\sigma$ in the second sum of the right-hand side of eq. (18) indicate the number of the element of a linearly stored lower triangle matrix; they are defined as $\varkappa\lambda = \frac{1}{2}\varkappa(\varkappa - 1) + \lambda$.

The expressions derived so far are valid not only for the energy gradient $\partial E^{B}_{\mathrm{elec}}/\partial q_a$, but also for $\mathbf{x}_1$ and $\mathbf{x}_2$, if the usual densities $\mathbf{Q}$ and $\mathbf{G}$ are replaced by difference densities in the case of $\mathbf{x}_1$ and by transition densities in the case of $\mathbf{x}_2$, respectively. As some terms disappear on forming the difference (for $\mathbf{x}_1$) or due to the orthogonality of the states A and B (in $\mathbf{x}_2$), it is useful to introduce the quantity

$$\delta_{AB} = \begin{cases} 1 & \text{for } \partial E/\partial \mathbf{q}, \\ 0 & \text{for } \mathbf{x}_1 \text{ and } \mathbf{x}_2 \end{cases}$$

to get compact expressions that apply to all three types of gradients, $\partial E/\partial \mathbf{q}$, $\mathbf{x}_1$, and $\mathbf{x}_2$.

For the solution of the CPHF equations, the Lagrange matrix eq. (17) has to be known. Siegbahn[22] has shown that the required elements can be obtained by summing only over the active-space elements of the one- and two-electron density matrix. If indices p, q, r, and s denote frozen occupied MOs (f.o.), t, u, v, and w MOs of the active space (AS) and i, j, k, l, and m arbitrary MOs, the only nonvanishing elements of the Lagrange matrix are

$$X_{ip} = 2X^{\mathrm{i}}_{pi}\delta_{AB} + \sum_{tu}^{\mathrm{AS}} Q_{tu}\left[2(pi|tu) - (pt|iu)\right] \qquad (21)$$

and

$$X_{it} = \sum_{u}^{\mathrm{AS}} Q_{tu} X^{\mathrm{i}}_{iu} + 2 \sum_{uvw}^{\mathrm{AS}} G_{tuvw}(iu|vw) \qquad (22)$$

where

$$X^{\mathrm{i}}_{ij} = h_{ij} + \sum_{p}^{\mathrm{f.o.}} \left[2(ij|pp) - (ip|jp)\right] \qquad (23)$$

is the inactive Fock matrix.

Using the same arguments that led to simplification of the Lagrange matrix, the transformation of the one- und two-electron density matrices from an MO to an AO basis can be written as

$$Q_{\mu\nu} = Q^{\mathrm{a}}_{\mu\nu} + 2D^{\mathrm{i}}_{\mu\nu}\delta_{AB} \qquad (24)$$

and

$$\begin{aligned} G_{\mu\nu\rho\sigma} = {} & \sum_{tuvw}^{\mathrm{AS}} c_{\mu t} c_{\nu u} c_{\rho v} c_{\sigma w} G_{tuvw} \\ & + \left(2D^{\mathrm{i}}_{\mu\nu} D^{\mathrm{i}}_{\rho\sigma} - \frac{1}{2} D^{\mathrm{i}}_{\nu\rho} D^{\mathrm{i}}_{\mu\sigma} - \frac{1}{2} D^{\mathrm{i}}_{\mu\rho} D^{\mathrm{i}}_{\nu\sigma} \delta_{AB}\right) \\ & + D^{\mathrm{i}}_{\mu\nu} Q^{\mathrm{a}}_{\rho\sigma} + D^{\mathrm{i}}_{\rho\sigma} Q^{\mathrm{a}}_{\mu\nu} - \frac{1}{4}\left(D^{\mathrm{i}}_{\nu\rho} Q^{\mathrm{a}}_{\mu\sigma}\right. \\ & \left. + D^{\mathrm{i}}_{\nu\sigma} Q^{\mathrm{a}}_{\mu\rho} + D^{\mathrm{i}}_{\mu\rho} Q^{\mathrm{a}}_{\nu\sigma} + D^{\mathrm{i}}_{\mu\sigma} Q^{\mathrm{a}}_{\nu\rho}\right) \end{aligned} \qquad (25)$$

where

$$D^{\mathrm{i}}_{\mu\nu} = \sum_{p}^{\mathrm{f.o.}} c_{\mu p} c_{\nu p} \qquad (26)$$

is the inactive SCF one-electron matrix and

$$Q^{\mathrm{a}}_{\mu\nu} = \sum_{tu}^{\mathrm{AS}} c_{\mu t} c_{\nu u} Q_{tu} \qquad (27)$$

is the active CI one-electron density matrix.

The great advantage of eqs. (21), (22), and (25) is due to the fact that the summations and the storage of the **G** matrix involve only the active-space indices.

The total gradient $\partial E^B_{\text{tot}}/\partial \mathbf{q}$ is obtained by adding the nuclear–nuclear contribution to the electronic part $\partial E^B_{\text{elec}}/\partial \mathbf{q}$; for $\mathbf{x}_1$ and $\mathbf{x}_2$ the nuclear–nuclear contribution vanishes.

INTEGRAL DERIVATIVES

As the MNDO parametrization is based on atomic parameters only, and does not include any bond parameters, the only derivative expressions required are these for the overlap integrals, $\partial S_{\mu\nu}/\partial q_a$, and for the two-electron repulsion integrals, $\partial(\mu\nu|\rho\sigma)/\partial q_a$. For a local coordinate system, the latter are available in the MNDO approximation, for example, in the MOPAC code,[23] while the $\partial S_{\mu\nu}/\partial q_a$ over STOs are easily obtained from the standard integrals $A_n(x)$ and $B_n(x)$.[24] The transformation from the local to the molecular coordinate system is accomplished by the orthogonal matrix

$$\mathbf{U} = (U_{q'_i q_j}) = \begin{pmatrix} \frac{\Delta q_1}{R} & \frac{\Delta q_2}{R} & \frac{\Delta q_3}{R} \\ \frac{\Delta q_2}{R_{q_1 q_2}} & -\frac{\Delta q_1}{R_{q_1 q_2}} & 0 \\ \frac{\Delta q_1 \Delta q_3}{R R_{q_1 q_2}} & \frac{\Delta q_2 \Delta q_3}{R R_{q_1 q_2}} & -\frac{R_{q_1 q_2}}{R} \end{pmatrix} \qquad (28)$$

where the $\Delta q_i = q_{K,i} - q_{L,i}$ $(i = 1, 2, 3)$ denote the differences of Cartesian coordinates of atoms K and L, $R = (\sum_{i=1}^{3} \Delta q_i^2)^{1/2}$ is the radius and $R_{q_1 q_2} = (\sum_{i=1}^{2} \Delta q_i^2)^{1/2}$ its projection onto the q_1, q_2 plane. Due to spherical symmetry, the s orbitals do not have to be transformed, while for the p orbitals one has

$$\mathrm{p}_{q_i} = \sum_{j=1}^{3} U_{q'_j q_i} \mathrm{p}_{q'_j}. \qquad (29)$$

Dashed (′) quantities refer to the local, and undashed ones to the molecular coordinate system.

IMPLEMENTATION

A flow chart of the algorithm for the evaluation of the analytic MNDO(C)–CI gradient is shown in Scheme 1. As input data, the following data, from a preceding SCF–CI calculation are required: the LCAO–MO coefficients $c_{\mu i}$, the orbital energies ε_i, the SCF density matrix $(D_{\mu\nu})$, the one- and two-electron integrals h_{ij} and $(ij|kl)$ in the MO basis, as well as the CI coefficients C_I.

The one- and two-electron coupling coefficients Q^{IJ}_{tu} and G^{IJ}_{tuvw} needed for the reduced density matrices (e.g., $Q_{tu} = \sum C_I C_J Q^{IJ}_{tu}$ and $G_{tuvw} = \sum C_I C_J G^{IJ}_{tuvw}$ for the $\partial E/\partial q_a$ case) are obtained from the routine for setting up the CI Hamiltonian matrix; for storage space reasons it is important that only elements referring to active-space orbitals are needed. In summing over IJ all $Q^{I'J'}_{tu}$ and $G^{I'J'}_{tuvw}$ for given $I'J'$ and all superindices tu and $tuvw$ are kept in temporary arrays. The $Q^{I'J'}_{tu}$ and $G^{I'J'}_{tuvw}$ are multiplied by the actual $C_{I'}C_{J'}$ and added to the corresponding partial sums of the densities Q_{tu} and G_{tuvw}. These densities are needed only for the t, u, v, and w of the active space, for example, for calculating the elements X_{ip} and X_{it} of the Lagrange matrix according to eqs. (21) and (22).

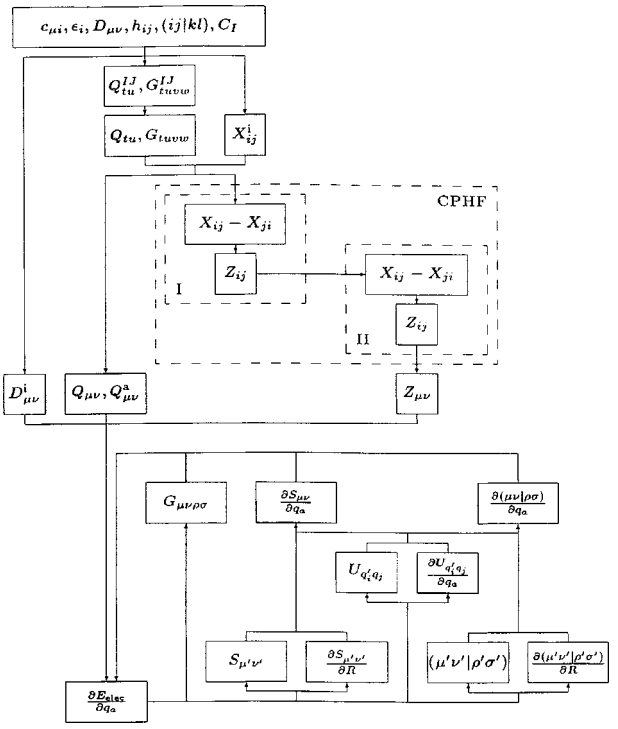

SCHEME 1. Flow chart of the analytic gradients routine for semiempirical ZDO calculations (I and II refer to the two subsets of CPHF equations).

From eqs. (21) and (22) it is apparent that the inactive Fock matrix X^{i}_{ij} of eq. (23) has to be evaluated for $i = t_{\min}, \ldots, t_{\max}$, $j = 1, \ldots, i$ as well as for $i = t_{\max} + 1, \ldots, N_{\text{orb}}$, $j = 1, \ldots, t_{\max}$, where $t_{\min}$ is the lowest and $t_{\max}$ the highest of the active space orbitals, and N_{orb} is the total number of MOs.

After these preliminaries the two subsets eqs. (13) and (14) of the CPHF equations can be solved. The resulting **Z** vector in MO basis is transformed into an AO basis according to eq. (19). After evaluating the inactive SCF density matrix eq. (26), one-electron density matrices are determined according to eqs. (24) and (27), and the loop for summing

up the analytic CI gradient, as given in this article explicitely only for the response term eq. (18), is executed. It runs over the AOs of all pairs of atoms K and L and over all Cartesian coordinates q_a ($a = 1, \ldots, 3N_{\text{atom}}$; N_{atom} is the number of atoms). To prevent extreme usage of internal storage, the two-electron density matrix $G_{\mu\nu\rho\sigma}$ as well as the derivatives of the overlap and the two-electron repulsion integrals $\partial S_{\mu\nu}/\partial q_a$ and $\partial(\mu\nu|\lambda\sigma)/\partial q_a$, respectively, are evaluated within the loop as well as the required quantities in the local (dashed) coordinate system and the transformation matrix and its derivative.

All four-index transformations are carried out by decomposing the fourfold sum into four single sums using the Diercksen algorithm.[25]

Although the solution $Z_{ij} = (X_{ij} - X_{ji})/(\varepsilon_j - \varepsilon_i)$ of subset I of the CPHF equations is trivial, the dimension of the matrix $\boldsymbol{\Delta}^{\text{II}} - \boldsymbol{\alpha}^{\text{II,II}}$ can become very large, and subset II is solved iteratively by conjugated gradient (CG) methods,[13] in which the matrix $\mathbf{A}$ of the linear system $\mathbf{Ax} = \mathbf{b}$ enters the calculation only by multiplication with a vector. Such a technique is applicable only if the matrix elements are easily accessible. Although Patchkovskii and Thiel[15] use an efficient symmetric formulation of the Z-vector method, the procedure used here is based on the preconditioned biconjugated gradient (PCBC) method, which does not require $\mathbf{A}$ to be symmetric or positive definite. The CPHF equations are usually diagonially dominant;[27] therefore, in agreement with common practice, the diagonal part of the matrix of coefficients in eq. (14) is chosen as a preconditioner to transform the linear system into the preconditioned form $(\tilde{\mathbf{A}}^{-1}\mathbf{A})\mathbf{x} = \tilde{\mathbf{A}}^{-1}\mathbf{b}$ to improve convergence of the iterative scheme.

The evaluation of $\boldsymbol{\alpha}^{\text{II,II}}$ is very fast, if the two-electron integrals in the MO basis required for $\boldsymbol{\alpha}^{\text{II,II}}$ are stored internally. If, however, the AO integrals have to be transformed into the MO basis, or if the integrals are kept in external storage, the iterative procedure has to be replaced by a conventional method, and the complete matrix has to be kept in the internal storage.

PERFORMANCE

The efficiency of our implementation of analytic gradients relative to the previous version of our MNDOC–CI program, where CI derivatives were found numerically, was tested choosing as in ref. 20 a number of cyclic polyethers $(CH_2OCH_2)_n$ with n ranging from 1 (oxirane) to 6 (18-crown-6). In each case the geometry was first optimized at the SCF closed-shell HF level; single-point calculations where then carried out for the energy and derivatives of the energy for the lowest excited singlet state. Convergence limits for the SCF procedure and the iterative solution of the CPHF equations were set to $\Delta_{\text{SCF}} = 10^{-8}$ kcal mol^{-1} and $\Delta_{\text{CPHF}} = 10^{-6}$. Extensive tests had shown that in general $\Delta_{\text{SCF}} = 10^{-5}$ kcal mol^{-1} and $\Delta_{\text{CPHF}} = 10^{-5}$ is sufficient to achieve an accuracy of 10^{-4} kcal (mol Å)$^{-1}$ for the energy gradients. The times (seconds of CPU time) required for calculating energies and derivatives both numerically and analytically are shown in Table I. The mean deviation ΔG of the Cartesian coordinates of the numerical and analytic gradients is smaller than $8 \cdot 10^{-3}$, and varies irregularly with the size (n) of the molecule. The time required to evaluate the analytic gradients G_{an} includes also the transformation of those two-electron integrals into the MO basis, which are not needed for the CI energy, for which according to the Stewart procedure[23] only integrals $(tu|vw)$ over active-space MOs and $(pp|qq)$, $(pq|pq)$ over frozen orbitals are needed, while the analytic gradients require all integrals over the complete orbital space. The time-determining steps in the evaluation of analytic gradients are the solution of the CPHF equations as well as the transformation of two-electron integrals from AOs to MOs and of the two-electron density matrix from MOs to AOs. Out of 168.43 s needed for G_{an} of the system with $n = 4$ the solution of the 1008×1008 system of CPHF equations takes 83.62 s (49.6%), while the transformation of the integrals and the density matrix require 42.17 s (25.0%) and 37.28 s (22.1%), respectively.

The excellent performance obtained by Patchkovskii and Thiel[14] for large molecules with minimal CI is not reached by the present implementation, which is designed for a CI encountered in treating photochemical reactions and conical intersections of medium-size molecules. As the accurate description of excited-state potential energy surfaces requires typically a CI expansion with several hundred configurations, the scaling with the size of the active space is more important than the scaling with the size of the system.

In Table II, the times required for gradient calculations for $(CH_2OCH_2)_2$ are listed for various choices of the active space. The ratio G_{num}/E is nearly constant and approximately equal to 80, while G_{an}/E decreases from 11.5 to 1.2 if the active space is changed from 1-1′ to 6-6′, where the occupied MOs of the ground configuration Φ_0 are numbered $1, 2, \ldots$, starting from the HOMO, and the unoccupied MOs by $1', 2', \ldots$, starting from the LUMO. The larger the active space, the faster the

TABLE I.
CPU Times (in Seconds) for Single-Point MNDOC–CI Calculations[a] of Energies *E*, and Numerical and Analytic Gradients G_{num} and G_{an} for the Series $(CH_2OCH_2)_n$ from Oxirane ($n = 1$) to 18-Crown-6 ($n = 6$).

n	N_{Orb}[b]	F[c]	E	G_{num}	G_{num}/E	G_{an}	G_{an}/E	G_{num}/G_{an}	ΔG[d]
1	16	21	2.34	83.04	35.5	2.63	1.1	31.6	$8.8 \cdot 10^{-4}$
2	32	42	3.62	280.89	77.6	16.77	4.6	16.7	$5.4 \cdot 10^{-3}$
4	64	84	12.17	1977.37	162.5	168.43	13.8	11.7	$4.9 \cdot 10^{-4}$
5	80	105	20.99	4405.54	209.9	389.37	18.6	11.3	$9.4 \cdot 10^{-4}$
6	96	126	37.12	9037.28	243.5	837.67	22.6	10.8	$7.9 \cdot 10^{-3}$

[a] All single and double excitations within the active space 4-4′, yielding a total of 153 CSFs.
[b] Number of basis-set AOs.
[c] Number of Cartesian coordinates.
[d] Average deviation of the Cartesian coordinates for numerical and analytic gradients in kcal (mol Å)$^{-1}$.

analytic gradient relative to the numerical one: the ratio G_{num}/G_{an} increases from 6.9 to 65.6 for the series of calculations shown in Table II.

Applications

The optimization procedure for conical intersections was tested for some model potentials and applied to locate the lowest energy points of the conical intersections in the photoreactions of ethylene and butadiene, for which *ab initio* data are available, before conical intersections of some systems that have not yet been treated were determined. Appropriate values for the scaling parameter of eq. (4) as well as for the parameter of eq. (6) were determined by testing the performance for selected model potentials and real molecules. The results described below were obtained by choosing $\alpha_0 = \alpha_1 = 0.01$ and $r = R = 0.1$ Å.

In Table III and Figure 2a results are shown for the S_1/S_0 conical intersection of ethylene. From Figure 1a it is seen that at the beginning the partial gradient $\mathbf{f}_1$ in the direction of the gradient difference vector dominates the optimization until after 11 iterations $E(S_1) \approx E(S_0)$; at this point (cf. Table III) the norm of the projected gradient $|\mathbf{f}_2| = 60.4$ kcal (mol Å)$^{-1}$ is still fairly large (Fig. 1b). In the following iterations $|\mathbf{f}_2|$ as well as $E(S_1)$ and $E(S_0)$ decrease steadily, the process being very similar to a geometry optimization with a poor initial geometry; the usual update procedure for the Hessian, like the BFGS method[13] used here, thus perform well. The optimized structure is in very good agreement with the *ab initio* data based on CASSCF calculations with an extended basis. Similar results were obtained for the S_1/S_0 conical intersection of the ethylene photodimerization reactions (Fig. 2b), where the values $\alpha = 20.8°$ and $R = 1.92$ Å (angle of rhomboidal

TABLE II.
CPU Times (in Seconds) for Single-Point MNDOC–CI Calculations[a] of Energies *E*, Numerical and Analytic Gradients G_{num} and G_{an} for (CH_2OCH_2) from Different Active Spaces AS.

AS	N_{conf}[b]	E	G_{num}	G_{num}/E	G_{an}	G_{an}/E	G_{num}/G_{an}	ΔG[c]
1-1′	3	0.63	49.95	79.3	7.25	11.5	6.9	$5.9 \cdot 10^{-3}$
2-2′	15	0.64	51.30	80.2	8.00	12.5	6.4	$4.6 \cdot 10^{-4}$
3-3′	55	1.00	77.58	77.6	10.50	10.5	7.4	$6.0 \cdot 10^{-3}$
4-4′	153	3.62	280.89	77.6	16.77	4.6	16.7	$5.4 \cdot 10^{-3}$
5-5′	351	11.79	919.74	78.0	31.83	2.7	28.9	$6.5 \cdot 10^{-3}$
6-6′	666	51.18	4029.17	78.7	61.42	1.2	65.6	$5.9 \cdot 10^{-3}$

[a] All single and double excitations within the given active space, except for AS 6-6′, where out of 704 CSFs only the 666 energetically lowest ones were included.
[b] Number of configurations.
[c] See Table I.

TABLE III.
Geometry Parameters of the Conical Intersection of the *cis-trans* Isomerization of Ethylene (Distances in Å, Angles in Degrees, Energies in kcal mol^{-1}).

Parameter	Start	At $E(S_1) \approx E(S_2)$	Minimum	Ref. 28 MNDOC–CI	Ref. 28 CASSCF[a]
C_1C_2	1.380	1.457	1.399	1.393	1.405
H_2C_1	1.300	1.360	1.232	1.240	1.221
$H_2C_1C_2$	60.9	55.3	73.9	73.1	77.2
$H_1C_1H_2C_2$	191.5	242.0	240.9	235.1	
$H_1C_1C_2H_3$	19.6	81.1	36.8	26.1	
$H_2C_1C_2H_3$	344.4	298.0	302.8	290.1	301.8
$E(S_1)$	203.5	151.2	116.5	122.5	

[a] *Ab initio* CAS (6,6) calculations, 6-31G** basis set.

distortion α and the distance R between the two parallel ethylene units) are again in good qualitative agreement with the *ab initio* values $\alpha = 25.5°$ and $R = 2.06$ Å of Bernardi et al.[29]

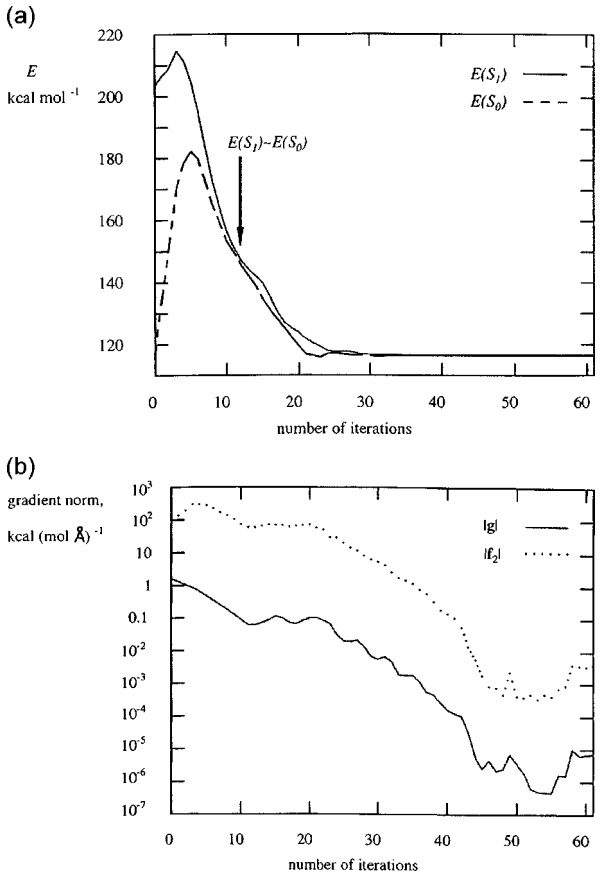

FIGURE 1. Optimization of the S_1/S_0 conical intersection of ethylene: (a) evolution of the state energies $E(S_1)$ and $E(S_0)$; (b) evolution of the norms of the total gradient **g** and of the projected gradient $\mathbf{f}_2$.

As a more severe test, the S_1/S_0 conical intersection of butadiene was chosen, which exhibits three minima in the intersections space.[30] The data in Table IV shows that not only three minima with CCCC dihedral angles of 45.2°, 74.0°, and 122.2°, which correspond to Olivucci's *s-cisoid*, *central*, and *s-transoid* minimum,[30] respectively, could be recovered by the semiempirical calculations, but that even the energetic ordering with the *s-transoid* minimum at lowest and the *central* minimum at highest energies has been retrieved. These results demonstrate that the algorithm implemented in our program is well suited also to treat complex topologies

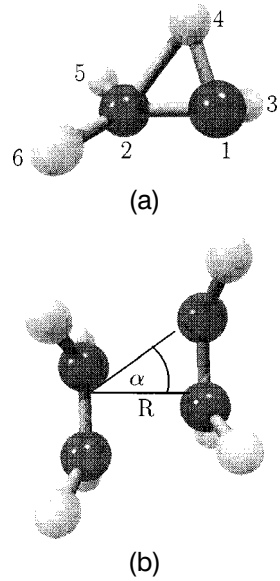

FIGURE 2. Conical intersections of ethylene photoreactions: (a) *cis-trans* isomerization (AS: 6-6′, ref. config.: Φ_0; 393 CSFs), and (b) dimerization (AS: 4-4′; ref. config.: Φ_0, $\Phi_{1\text{-}1'}$, $\Phi^{1\text{-}1'}_{1\text{-}1'}$, $\Phi^{1\text{-}2'}_{1\text{-}2'}$; 426 CSFs).

TABLE IV.
Geometry Parameters, Energies, and Gradient Norm $|f_2|$ of the Conical Intersections (CI) of Butadiene [Distances in Å, Angles in Degrees, Energies in kcal mol^{-1}, Gradients in kcal (mol Å)$^{-1}$].[a]

Parameter	*Central* CI		*s-cisoid* CI		*s-transoid* CI	
C_1C_2	1.439	[1.48]	1.447	[1.51]	1.436	[1.47]
C_1C_3	2.029		2.491		2.043	
C_2C_3	1.433	[1.47]	1.419	[1.39]	1.426	[1.41]
C_2C_4	2.603		1.923		2.522	
C_3C_4	1.454	[1.48]	1.439	[1.47]	1.443	[1.48]
$C_1C_2C_3C_4$	74.0	[84]	45.2	[52]	122.0	[119]
$H_6C_1C_2H_7$	139.1	[146]	13.3	[40]	38.5	[34]
$H_{10}C_4C_3H_8$	109.9	[83]	130.1	[143]	69.0	[73]
$\Delta E(S_1)$[b]	6.4	[9.3]	5.8	[6.8]	0	[0]
$\|\mathbf{f}_2\|$	$4.9 \cdot 10^{-4}$		$3.0 \cdot 10^{-4}$		$3.0 \cdot 10^{-4}$	
$E(S_1) - E(S_0)$	$6.0 \cdot 10^{-5}$		$3.3 \cdot 10^{-6}$	[0.31]	$3.4 \cdot 10^{-6}$	[0.06]

[a] *Ab initio* values in brackets from ref. 29.
[b] Energy relativ to the *s-transoid* CI.

(three critical points within one intersection space) as well as the fact that the semiempirical MNDOC–CI method is able to produce meaningful results even for such difficult situations; it is, therefore, particularly useful for the preliminary determination of larger areas of excited-state potential energy surfaces, which may provide detailed insight into the mechanism of photochemical reactions, even of complex systems.[31]

In the case of 2,3-di-*t*-butylbutadiene, only one critical point could be found in the intersection space. The geometry at this conical intersection (Fig. 3a) corresponds to the *s-transoid* minimum (Fig. 3b) in the intersection space of butadiene; it is characterized by a particularly small 1,3-distance. It is, thus, not surprizing, that in the presence of 2,3-di-*t*-butyl substituents the corresponding bicyclo[1.1.0]butane, which is usually a minor side product of the butadiene photocyclization, becomes the major photoproduct.[32]

For 2H-azirine, the two conical intersections shown in Figure 4 could be located. At the S_2/S_1 conical intersection (Fig. 4a) the CN double bond is considerably elongated; in a barrierless S_1 reaction a nitrene can be formed, which either can deacti-

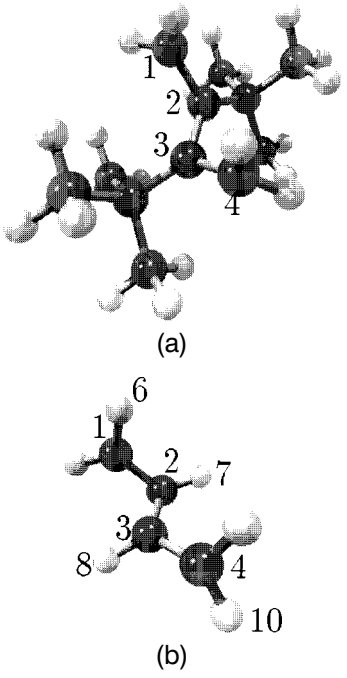

FIGURE 3. (a) Conical intersections of 2,3-di-*t*-butyl butadiene (AS: 2-2′; ref. config.: Φ_0, $\Phi_{1\text{-}1'}$, $\Phi^{1\text{-}1'}_{1\text{-}1'}$, $\Phi^{1\text{-}2'}_{1\text{-}2'}$; 20 CSFs) and (b) the *s-transoid* conical intersection of butadiene (AS: 2-2′; ref. config.: Φ_0, $\Phi_{1\text{-}1'}$, $\Phi^{1\text{-}1'}_{1\text{-}1'}$, $\Phi^{1\text{-}2'}_{1\text{-}2'}$; 20 CSFs).

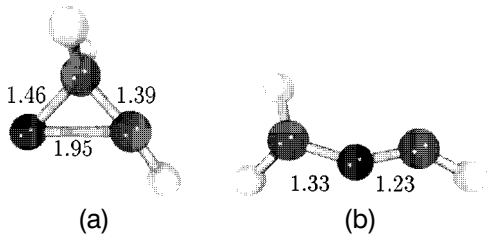

FIGURE 4. Conical intersections of azirine: (a) S_2/S_1 conical intersection (AS: 5-4′; ref. config.: Φ_0, $\Phi_{2\text{-}1'}$; 489 CSFs), and (b) S_1/S_0 conical intersection (AS: 3-2′; ref. config.: Φ_0, $\Phi_{1\text{-}1'}$, $\Phi^{1\text{-}1'}_{1\text{-}1'}$; 43 CSFs).

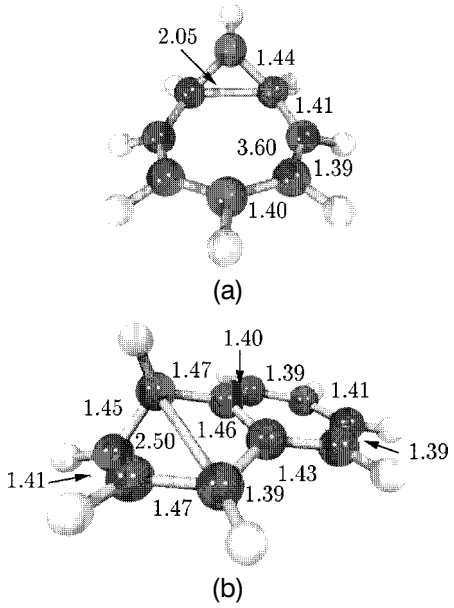

FIGURE 5. Conical intersections of (a) the cyclo-octatetraene – semibullvalene rearrangement (AS: 4-4′; ref. config.: Φ_0, $\Phi_{1\text{-}1'}$; 306 CSFs), and (b) the dewarnaphthalene – naphthalene rearrangement (AS: 3-3′; ref. config.: Φ_0, $\Phi_{1\text{-}1'}$; 55 CSFs).

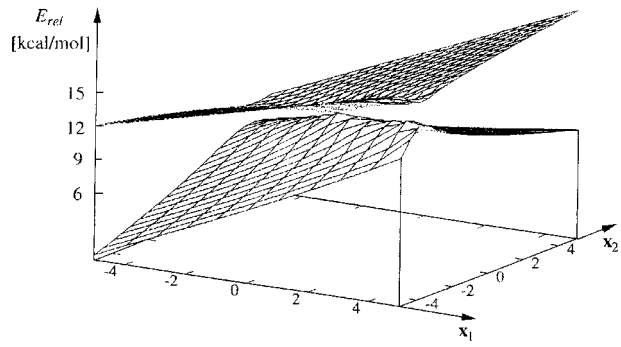

FIGURE 6. S_1 and S_0 potential energy surfaces at the conical intersection of dewarnaphthalene, plotted against the orthogonalized $\mathbf{x}_1$ and $\mathbf{x}_2$ vectors (in units of 10^{-2} amu^{-1} bohr).

vate back to ground-state 2H-azirine[33] or else can undergo ISC to form a triplet species. The S_1/S_0 conical intersection (Fig. 4b), on the other hand, corresponds to a CC bond rupture and the formation of a nitrile ylide, which is a highly reactive intermediate.[34] A detailed theoretical study of the photochemistry of 2H-azirine and its substitution products is at present underway.[35]

Figure 5a, finally, shows the S_1/S_0 conical intersection for the cyclooctatetraen-semibullvalene photorearrangement,[36] confirming that this is a direct photoconversion with no intermediate being involved. As suggested by Zimmerman,[36] both 1,5 and 4,6 bonding are developing simultaneously, with the 4,6 distance, however, being considerably shorter than the 1,5 distance. The detailed reaction path from the Franck–Condon region toward the conical intersection has yet to be investigated to determine the influence of the cyclooctatetraen conformation. In Figure 5b, the S_1/S_0 conical intersection for the dewarnaphthalene–naphthalene rearrangement is shown. This reaction has been studied in great detail by Wallace and Michl,[37] who found a 14% probability of an diabatic reaction to form S_1-excited naphthalene. This experimental finding can be understood on the basis of the shape of the excited-state potential energy surface, which is very steep with the conical intersection 44.2 kcal mol^{-1} below the Franck–Condon geometry and 23.9 kcal mol^{-1} above that of naphthalene. Near the conical intersection, however, it is very flat, and the funnel is poorly developed (Fig. 6); thus, quite a number of trajectories will miss the conical intersection and continue to the spectroscopic minimum of naphthalene. More detailed investigations of this situation are underway.[38]

Conclusion

The analytic gradients for semiempirical MR–CI calculations derived in this article represent a very powerful and efficient tool for the determination of excited state potential energy surfaces, and in particular, for locating conical intersections.[39] The analytic gradients make geometry optimizations faster by a factor of approximately 60, depending on the size of the molecule, and especially the size of the CI. The method is thus especially suited for a theoretical discussion of the mechanisms of photochemical reactions, as molecules as large as dewarnaphthalene or di-*t*-butylbutadiene can be treated quite easily, and further improvements of the performance are possible[14] and underway. One is, therefore, not restriced to discuss model systems, and systematic studies of structural variations and substituent effects are well within reach. Such studies can be very useful, as all essential features of the excited-state potential energy surfaces are represented qualitatively correct on the semiempirical level of theory, and relative energies are reproduced quite well. To obtain absolute values for excitation energies or barrier heights, however, sophisticated *ab initio* calculations are required, for which the semiempirical results represent a good

starting point. Furthermore, the analytic gradients will make calculations sufficiently fast for "on the fly" determinations of excited-state trajectories.

Acknowledgments

Thanks are due to C. Bornemann, Dr. C. Hoinka, and T. Jödicke for their contributions to some of the calculations; to C. Wittekindt for the figures; and to Dr. U. Höweler for the introduction into the existing program and the assistance during the incorportation of the new routines.

References

1. Trushin, S. A.; Diemer, S.; Fuß, W.; Kompa, K. L.; Schmid, W.E. Phys Chem Chem Phys 1999, 1431.
2. Fuß, W.; Lochbrunner, S.; Müller, A. M.; Schikarski, T.; Schmid, W. E.; Trushin, S. A. Chem Phys 1998, 232, 161; Trushin, S. A.; Fuß, W.; Schikarski, T.; Schmid, W. E.; Kompa, K. L. J Chem Phys 1997, 106, 9386.
3. Bearpark, M. J.; Robb, M. A.; Schlegel, H. B. Chem Phys Lett 1994, 223, 269.
4. Garavelli, M.; Bernardi, F.; Olivucci, M.; Vreven, T.; Klein, S.; Celani, P.; Robb, M. A. Faraday Discuss 1998, 110, 51.
5. Bernardi, F.; Olivucci, M.; Robb, M. A. Chem Soc Rev 1996, 321.
6. Roos, B. O. Lecture Notes in Quantum Chemistry, Springer Verlag: Berlin, 1992.
7. Steuhl, H.-M.; Klessinger, M. J Chem Soc Perkin Trans 1998, 2, 2035.
8. Dreyer, J.; Klessinger, M. Chem Eur J 1996, 2, 335.
9. Thiel, W. J Am Chem Soc 1981, 103, 1413.
10. Klessinger, M.; Pötter, T.; v. Wüllen, C. Theoret Chem Acta 1991, 80, 1.
11. Ben-Nun, M.; Martinez, T. J Chem Phys Lett 1998, 298, 57.
12. Carpenter, B. K. Angew Chem Int Ed Eng 1998, 37, 3340.
13. Press, W. H.; Teukolsky, S. A.; Vetterling, W. T.; Flannery, B. P. Numerical Recipes, Cambridge University Press: Cambridge, 1992.
14. Patchkovskii, S.; Thiel, W. Theor Chem Acc 1997, 98, 1.
15. Patchkovskii, S.; Thiel, W. Theor Chim Acta 1996, 93, 87.
16. Shavitt, I. Methods of Electronic Structure Theory; Schaefer, H. F., III, Ed.; Plenum: New York, 1977, pp. 189–275.
17. Yamaguchi, Y.; Osamura, Y.; Goddard, J. D.; Schaefer, F., III A New Dimension to Quantum Chemistry: Analytic Derivative Methods in Ab initio Molecular Electronic Structure Theory; Oxford University Press, Inc.: New York, 1994.
18. Davidson, E. R. Reduced Density Matrices in Quantum Chemistry; Academic Press: New York, 1976.
19. Handy, N. C.; Schaefer, H. F., III J Chem Phys 1984, 81, 5031.
20. Dewar, M. J. S.; Liotard, D. A. J Mol Struct (Theochem) 1990, 26, 123.
21. Rice, J. E.; Amos, R. D.; Handy, N. C.; Lee, T. J.; Schaefer, H. F., III J Chem Phys 1986, 85, 963.
22. Siegbahn, P. E. M.; Almlöf, J. A.; Heiberg, A.; Roos, B. O. J Chem Phys 1981, 74, 2384.
23. Stewart, J. J. P. MOPAC 7.0, a General Molecular Orbital Package, QCPE 455, 1993.
24. Izzo, R. Thesis, Münster (1998).
25. Diercksen, G. H. F. Theoret Chem Acta 1974, 33, 1.
26. See ref. 13; for a discussion of preconditioning of CPHF equations for second derivatives of the energy in MNDO methods, see ref. 27.
27. Patchkovskii, S.; Thiel, W. J Comput Chem 1996, 17, 1318.
28. Freund, L.; Klessinger, M. Int J Quantum Chem 1998, 70, 1023.
29. Bernardi, F.; De, S.; Olivucci, M.; Robb, M. A. J Am Chem Soc 1990, 112, 1737.
30. Olivucci, M.; Ragazos, I. N.; Bernardi, F.; Robb, M. A. J Am Chem Soc 1993, 115, 3710.
31. Steuhl, H.-M.; Bornemann, C.; Klessinger, M. J Eur Chem 1999, 5, 2404.
32. Hopf, H.; Lipka, H.; Traetteberg, M. Angew Chem Int Ed Eng 1994, 33, 204.
33. Bock, H.; Dammel, R.; Aygen, S. J Am Chem Soc 1983, 105, 7681.
34. Padwa, A. Acc Chem Res 1976, 9, 371.
35. Bornemann, C. Thesis, Münster (1999).
36. Zimmerman, H. E.; Iwamura, H. J Am Chem Soc 1970, 92, 2015.
37. Wallace, S. L.; Michl, J. Photochem Photobiol; Proc. Int. Conf. Alexandria; Zewail, A. H., Ed.; 1983, pp. 1191–1196, vol. 2.
38. Jödicke, T.; Bornemann, C.; Klessinger, M. (in preparation).
39. This program is available on request from the authors.